topographic images or in the 'error signal' maps which can be more sensitive to small topographic features. We have made extensive searches with a considerable number of samples prepared on different occasions to confirm that the lack of visible topographic detail is characteristic of these patterned surfaces. In addition we took care to ensure that the stripes observed in the friction map are genuine. Using tips functionalized with a racemic mixture of the chiral ligand **T**, we searched for evidence of contrast in both the topographic and friction images (experiments were performed with six racemic tips). No contrast was found. This null result for a racemic tip is consistent with the measurements of adhesion, and it implies that there are equal numbers of *R* and *S* molecules of the resin on the tip within the contact region.

The results above show that chemical force microscopy is sufficiently sensitive to permit discrimination between enantiomers of simple chiral molecules. For the systems used here, there is a difference of essentially 100% in the pull-off force for different enantiomers, and this difference in adhesion displays itself in frictional contrast on enantiomerically patterned surfaces. The chiral discrimination observed in these experiments must arise solely from the different diastereomeric complexes transiently formed between the chiral molecule on the tip and either the *R* or *S* mandelic acid on the surface. (The retention times for homologues of our mandelic acid derivatives, on a HPLC column containing the resin used here, give the same pattern as for the adhesion forces.) In other CFM studies that purportedly demonstrate chemical discrimination there is topographic and frictional contrast arising from variation of the mechanical properties of the film caused by variation in the intermolecular packing in the self-assembled monolayer for differently functionalized surfaces. We have eliminated this artefact from our experiments by use of surface patterns that differ only in their handedness. The packing and interfacial free energies are the same for the enantiomers in each pair, as confirmed by measurements of contact angles.

Now that chiral discrimination through CFM has been demonstrated, the next step is to gain a quantitative understanding of the results at a molecular level. We are investigating the packing and orientation of the functional groups of the self-assembled monolayers by means of Fourier-transform infrared spectroscopy. Coupled with molecular modelling this should improve understanding of the differences between the derivatives **M1**, **M2** and **M3**. Explanation of the adhesion energies requires an appropriate mechanical model for the interactions between the tip and surface. Work has shown that the JKR model[5,9] of mechanical contacts is a good starting point for quantitative analysis of CFM[10], and therefore to test this model's applicability, we are measuring the tip radius by scanning and transmission electron microscopy, and the surface energies by contact angle measurements. In these experiments we have measured both adhesion and friction, and although there is a link between these, its nature is one of the outstanding problems in tribology[11]. From a qualitative chemical viewpoint it is clear that in these experiments the variation of friction between enantiomers must arise from the breaking of different diastereomeric complexes transiently formed in the region between chiral molecules on the tip and either the *R* or *S* mandelic acid on the surface. More experiments are being undertaken to improve the resolution and accuracy of the friction force maps[12].

The observation of chiral discrimination, which is fundamental to drug–target interactions, demonstrates that CFM can be used in the sophisticated way necessary to look for differential binding interactions between arrayed libraries of small molecules or oligonucleotides. In addition, experiments such as these may permit a step forward in our understanding of the subtle relationship between friction and adhesion, as they allow the interaction between the tip and surface to be changed without alteration of the mechanical properties of the surface or the wetting energies of tip or surface. □

Received 20 August; accepted 24 November 1997

1. Frisbie, C. D., Rozsnyai, L. F., Noy, A., Wrighton, M. S. & Lieber, C. M. Functional group imaging by chemical force microscopy. *Science* **265,** 2071–2074 (1994).
2. Lee, G. U., Kidwell, D. A. & Colton, R. J. Sensing discrete streptavidin–biotin interactions with atomic force microscopy. *Langmuir* **10,** 354–357 (1994).
3. Ludwig, M., Dettmann, W. & Gaub, H. E. Atomic force microscope imaging contrast based on molecular recognition. *Biophys. J.* **72,** 445–448 (1997).
4. Boland, T. & Ratner, B. D. Direct measurement of hydrogen bonding in DNA nucleotide bases by atomic force microscopy. *Proc. Natl Acad. Sci. USA* **92,** 5297–5301 (1995).
5. Israelachvili, J. Intermolecular and Surface Forces (Academic, New York, 1992).
6. Pirkle, W. H., Finn, J. M., Schreiner, J. L. & Hamper, B. C. A widely useful chiral stationary phase for the high-performance liquid chromatography separation of enantiomers. *J. Am. Chem. Soc.* **103,** 3964–3966 (1981).
7. Weis, R. M. & McConnell, H. M. Two-dimensional chiral crystals of phospholipid. *Nature* **310,** 47–49 (1984).
8. Stevens, F., Dyer, D. J. & Walba, D. M. Direct observation of enantiomorphous monolayer crystals from enantiomers by scanning tunneling microscopy. *Angew. Chem. Int. Edn Engl.* **35,** 900–901 (1996).
9. Johnson, K. L. Continuum mechanics of adhesion and friction. *Langmuir* **12,** 4510–4513 (1996).
10. Noy, A., Frisbie, C. D., Rozsnyai, L. F., Wrighton, M. S., Lieber, C. M. Chemical Force Microscopy: exploiting chemically-modified tips to quantify adhesion, friction and functional group distribution in molecular assemblies. *J. Am. Chem. Soc.* **117,** 7943–7951 (1995).
11. Yoshizawa, H., Chen, Y.-L. & Israelachvili, J. Fundamental mechanism of interfacial friction. I. Relation between adhesion and friction. *J. Phys. Chem.* **97,** 4128–4140 (1993).
12. Lantz, A. M., O'Shea, S. J., Welland, M. E. & Johnson, K. L. Atomic force microscope study of contact area and friction on $NbSe_2$. *Phys. Rev. B* **55,** 10776–10785 (1997).
13. Sader, J. E., Larson, I., Mulvaney, P. & White, L. R. Method for the calibration of atomic force microscope cantilevers. *Rev. Sci. Instrum.* **66,** 3789–3798 (1995).
14. Kumar, A. & Whitesides, G. M. Features of gold having micrometer to centimeter dimensions can be formed with an elastomeric stamp and an alkanethiol "ink" followed by chemical etching. *Appl. Phys. Lett.* **63,** 2002–2004 (1993).

Acknowledgements. We thank S. O'Shea for discussions, G. Whitesides (Harvard University) and H. Bieybuck (IBM Zurich) for providing microcontact stamps, and R. Mellor for programming. We acknowledge financial support from Zeneca for a studentship (R.A.M.), and EPSRC for a postdoctoral fellowship (M.-E.T.).

Correspondence and requests for materials should be addressed to T.R. (e-mail: tr22@cam.ac.uk).

Spontaneous assembly of marine dissolved organic matter into polymer gels

Wei-Chun Chin, Mónica V. Orellana & Pedro Verdugo

Department of Bioengineering, University of Washington, Box 357962, Seattle, Washington 98195, USA

A large pool of organic carbon resides in the world's oceans in the form of dissolved organic matter (DOM)[1,2]. DOM is operationally defined as the fraction of organic matter that passes through a filter with a given pore size (which can range from less than 0.1 μm to 0.46 μm). This fraction has a longer oceanic residence time—and is generally less biodegradable—than particulate organic matter (POM)[1–4]. Processes transforming DOM into POM are therefore crucial for our understanding of the cycling of organic material in the oceans[1–4]. The aggregation of marine colloids, which constitute 10–40% of DOM[2,3,5], is thought to be an important step in the transformation of DOM into POM[3]. It has been suggested that colloids, as well as transparent exopolymer particles and large aggregates ('marine snow') can be viewed as polymer gels[6–8]. Whether free DOM polymers can indeed spontaneously assemble to form polymer gels has, however, not yet been shown. Here we present experimental observations that demonstrate that marine polymer gels can assemble from free DOM polymers, and that their formation mechanism, physical characteristics and mineralization can be understood in terms of polymer gel theory[9–11]. The principles and methods of polymer gel physics thus have the potential to provide profound new insights into the processes controlling the exchange between the DOM and POM pools and the cycling of marine organic matter.

Polymer gels are formed by a three-dimensional polymer network and a solvent which in the case of hydrogels is water. Although the

solvent prevents the collapse of the network, the network entraps the solvent, creating a micro-environment that is in thermodynamic equilibrium with the surrounding media. The polymer chains that form the network are interconnected by chemical or physical crosslinks and thus stay in a statistically stable neighbourhood. Depending on the characteristics of the polymer chains (such as polyelectrolytic properties, degree of hydrophobicity, length, linear or branched chains), and the dielectric properties of the solvent, the polymers in the gel's matrix can interact strongly with each other, with the solvent, or with smaller solutes. These interactions determine the gel's physical properties. The study of polymer gels is an active area of research in modern physics, and here we use the insights gained in such studies to investigate the processes affecting marine organic matter.

The kinetics of DOM polymer assembly were monitored by measuring particle size as a function of time using dynamic laser scattering spectroscopy (DLS) and flow cytometry (Fig. 1a). Results show that DOM polymers in 0.22 μm-filtered sea water from Puget Sound, the North Pacific Ocean and the Arctic Ocean, can spontaneously assemble, forming polymer gels ranging from colloidal to micrometre size. In these experiments sea water suffered no processing other than gentle gravity filtration. DLS shows that fresh filtrate contains a polydisperse set of polymers with sizes ranging from 2 to 200 nm. About 30 minutes after filtration, DLS reveals the presence of a polydisperse collection of assembled polymer gels (POM) ranging in size from 200 nm to 1 μm. The assembly process is nonlinear and the increase in particle size follows a sigmoidal course resembling second-order kinetics. Independent measurements of particle size as a function of time, performed in replicate samples using flow cytometry, reveal a similar pattern of assembly. Both methods show that microgels continue growing for the next 50 h, reaching an average equilibrium size of ~5 μm in 50–83 h. These techniques provide independent evidence that DOM polymers can undergo rapid spontaneous assembly into POM particles which, as shown below, have the typical features of polymer gels.

A control experiment showed that the assembly of microgels in sea water filtered either once or twice (with a period of 8 days between the two filtrations) follows, within experimental error, the same time course. These results, together with environmental scanning electron microscopy (ESEM) observations that microgels are retained intact by the filter (Fig. 3, inset a), confirm that gravity filtration gently removes the microgels. As the assembly kinetics are concentration dependent, the observation also suggests that only a small fraction of the free DOM polymers forms microgels. This is in agreement with recent studies[2,12] which suggest that only ~10% of DOM is transformed into POM.

The equilibrium particle size of the assembled gels depends on the total amount of available free polymers. Because there is a finite amount of polymers in the 10-ml samples, the average equilibrium size of microgels is only ~5 μm. But in the ocean, with a virtually infinite source of free polymers, the gels could potentially reach larger sizes.

Flow cytometry reveals that while the concentration of microgels decreases exponentially, their average size undergoes a corresponding increase (Fig. 2). These measurements, together with the sigmoidal time course of increase in particle size (Fig. 1a), imply that the formation and growth of marine microgels result both from the continuous assembly of free polymers into microgels and from secondary aggregation and annealing of small assembled gels. This is further supported by the observation that in each of the three replicates tested the total volume of gel remains constant over the time course of assembly.

Divalent bonds are known to stabilize the matrix of polyanionic gels[13]. In the case of marine hydrogels, chelation of Ca^{2+} and Mg^{2+} by addition of 10 mM ethylenediamine-tetra-acetic acid (EDTA) to the sea water inhibits polymer assembly (Fig. 1a). Furthermore, EDTA can readily disperse marine microgels, releasing free polymers of about 1 to 2.5 nm in size. This size range is known to be the main fraction of DOM[2,14]. Dispersion induced by EDTA provides evidence that the polymer matrix of these gels is an ionic-bond-stabilized tangled network, rather than a covalently crosslinked network. The presence of bound Ca^{2+} inside the microgels was

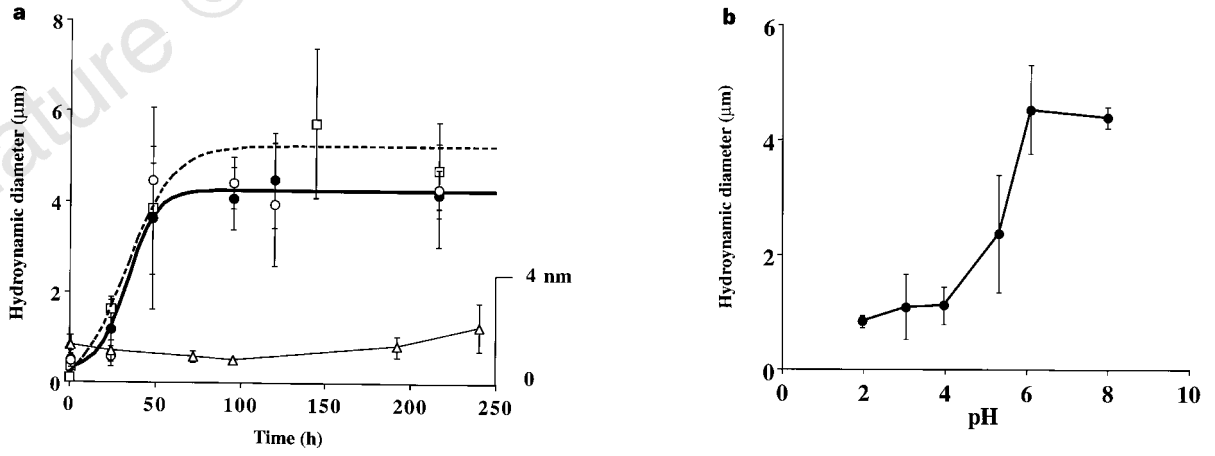

Figure 1 Polymer gel size as a function of assembly time and pH. **a**, The assembly of polymer gels was monitored by measuring particle size by both homodyne dynamic laser scattering (filled circles, solid line), and by flow cytometry (empty squares, dashed line). Parallel measurements were conducted in sea water containing 0.02% sodium azide (empty circles) to inhibit microbial activity. Control experiments in which the polymer assembly was inhibited by chelating Ca^{2+} and Mg^{2+} by addition of 10 mM EDTA to the sea water gave an average size of 1–2.5 nm, regardless of the time of observation (empty triangles, solid line). Measurements of microgel size by flow cytometry and DLS show a similar time course of assembly. We note that, depending on assembly time, the size of assembled polymer gels ranges from colloidal, submicrometre size, to several micrometres. Each point corresponds to the average ± s.d. of five measurements made on three replicate samples of sea water. **b**, Experiment showing that marine polymer gels can undergo a fast (<1 min) swelling/condensation transition from hydrated to condensed phase by changing the pH of the sea water. The size of the gels was monitored by DLS, and also verified by optical microscopy (data not shown). The swelling/condensation transition is reversible, and has a steep sigmoidal change in the volume of the gels that reflects the characteristic high apparent cooperativity of this phenomenon. Each point corresponds to the average ± s.d. of five measurements made on three replicate samples of sea water. Measurements by flow cytometry performed in the same samples showed no statistical difference in the concentration of microgels in swollen or condensed phase.

revealed by chlortetracycline stain[15] (Fig. 3 inset b). Calcium partition inside the gels is likely to result from a Donnan equilibrium due to the polyanionic nature of their polymer matrix[8,16–18]: at the normal pH of the sea water (pH 8.2), calcium attached to the gel matrix does not crystallize. But because the concentration of Ca^{2+} inside the gels must be higher and closer to critical saturation than the concentration of Ca^{2+} in sea water, slight increases of pH that do not produce precipitation in sea water can result in crystalline mineralization of the gel's matrix. Polyanion-mediated formation of mineral–polymer composites has been observed inside alginate microgels[19], in the Golgi of coccolithophorid algae[20], and in other biomineralization processes[18,21]. Hence, increased pH in sea water (8.5 to 9)—as found in microenvironments during high productivity[22]—could induce crystalline mineralization of marine microgels. Crystalline mineralization could result in increased sedimentation rate, and may account for the formation of calcified aggregates and sediments (Fig. 4), such as mineral grains in marine aggregates, mineral-based marine snow, whitings and ooids[6,23]. In hydrated microgels, polarization microscopy also reveals the presence of crystalline structures (data not shown). X-ray microanalysis (Fig. 3) indicates that this crystalline mineral–polymer composite is rich in calcium and low in phosphorus, suggesting the presence of calcium carbonate rather than calcium phosphate.

Images of fully hydrated gels were obtained by ESEM; (Fig. 3 inset a). This method complements the DLS and flow cytometry measurements, providing a precise, independent validation of the size of the gels. It also serves as a control for microbial contamination and for artefacts produced by other traditional electron microscopy methods that require chemical fixation. Histochemical staining with alcian blue, Ponceau S, Schiff stain, lectins, Nile red and fluorescently labelled antibodies against ribulose-1,5-biphosphate carboxylase/oxygenase (Rubisco)[24], indicate that the polymer matrix of these microgels contains carbohydrates, proteins (Rubisco) and lipids (data not shown).

A typical feature of all polymer gels is that they can undergo

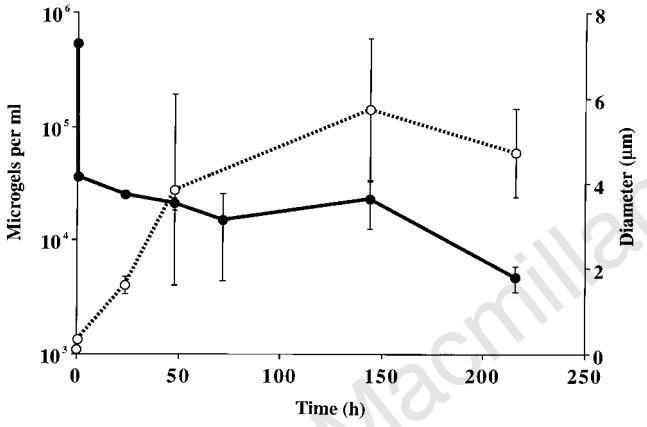

Figure 2 The concentration and size of marine microgels as a function of time of assembly. Data were obtained by flow cytometry in three replicates of 0.22-μm-filtered Puget Sound sea water. Although size increases (empty circles), the particle concentration in the sea water shows a corresponding decrease (filled circles). Because the volume of a particle is proportional to the cube of its diameter, the initial decrease of particle concentration should not be accompanied by a significant increase in particle size. The rate of decrease in microgel concentration is therefore expected to be faster than the rate of increase in microgel diameter. Each point corresponds to the average ± s.d. of two measurements on three replicate samples of sea water.

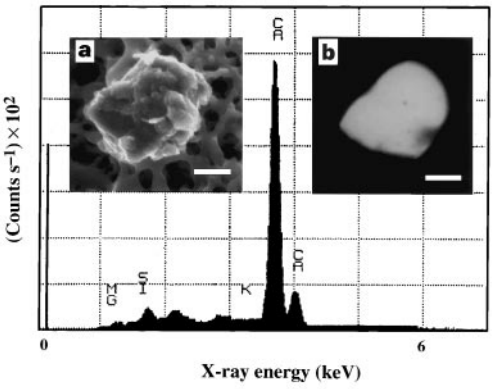

Figure 3 Averaged X-ray spectra showing the elemental composition inside a marine microgel. We note the large peak of calcium and the absence of phosphorus. Inset a shows an ESEM micrograph of a hydrated marine microgel (scale bar, 2 μm). Inset b reveals the presence of bound calcium in a microgel stained with chlortetracycline (scale bar, 2 μm).

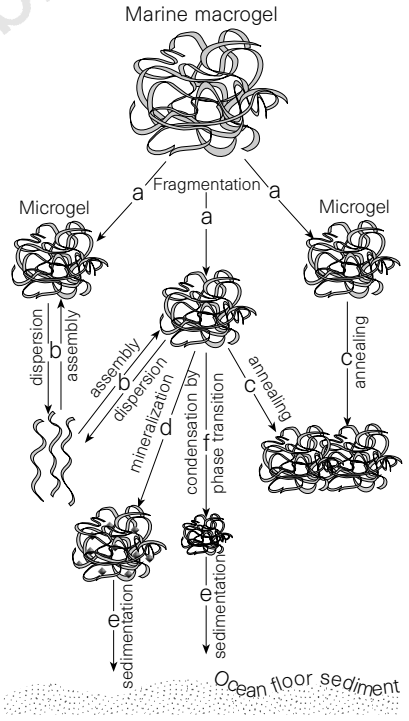

Figure 4 Processes transforming free marine polymers and polymer gels. Marine polymer microgels can result from partial fragmentation of gels secreted by phytoplankton or other organisms (a), or from assembly of free marine polymer (DOM) (b). The process of assembly is reversible, and microgels can be readily redispersed via physical, chemical or biological processes (b). Marine microgels can aggregate, and due to their tangled topology they can also 'anneal' to each other, forming larger stable polymer gels (c). Annealing is the process whereby polymers from one gel can diffuse and interpenetrate neighbouring gels, forming larger, interwoven networks. Because of their polyanoionic properties, marine microgels concentrate calcium and can undergo crystalline mineralization (d), increasing their density and sedimentation rate (e). A less likely outcome in the ocean, but one that cannot be ruled out *a priori* is that microgels could undergo polymer gel phase transition by high pressure, low temperature and/or the presence of organic pollutants (f). The resulting high density of condensed microgels could also increase their vertical flux to the sediment (e). Both crystalline mineralization and/or condensation could potentially make microgels refractory to biodegradation.

reversible phase transitions from condensed to hydrated phases[11]. By lowering the pH to 4.5 the microgels described here can also undergo a swelling/condensation transition from hydrated to condensed phase, as revealed by their volume change. The process is reversible and shows high apparent cooperativity, as shown by the steep sigmoidal swelling/condensation transitions depicted in Fig. 1b. The finding that condensation of marine polymer gels takes place at pH 4.5, the pK_a of carboxylic acid groups, is consistent with observations indicating that one out of every six carbon residues in DOM corresponds to a carboxylic group[25]. These phase transition experiments were not designed to imitate conditions found in the ocean but to demonstrate the polymer gel nature of the networks assembled from DOM polymers. However, polymer gel phase transitions can be triggered by a variety of stimuli that may be relevant to the ocean, including high pressure, low temperature, or the presence of organic pollutants. The effect of these environmental conditions remains to be studied. When hydrogels undergo phase transition, their polymer network collapses into a dense, nonporous array that can exclude (or entrap) species of relative molecular mass as low as 300–500 (ref. 19). Biodegradable species can become refractory by forming, or by being entrapped in, microgels that exclude bacteria or enzymes via topological hindrance[26,27]. Diffusional exclusion has been proposed to explain the unusual diagenetic stability of algaenans (algae-derived organic matter) and their high efficiency as carbon sinks[28]. Condensation can also increase the density and sedimentation rate of these gels, providing an additional route for their removal from the water column (Fig. 4).

The present data show that without chemical reactions DOM polymers can entangle spontaneously to form POM microgels. According to Edward's theory (ref. 10), the probability of spontaneous assembly of tangled (non-covalently crosslinked) networks and the stability of these networks increase with the second power of the polymer length[10]. The dynamics of assembly of polymers in sea water, which contains longer chains than those only from the DOM pool, should therefore be faster, and the assembled gels should be more stable. Conversely, the breaking of marine polymers by ultraviolet photolysis[29] or by enzymatic degradation results in progressively shorter chains and correspondingly unstable gels. Polymer gel theory[10] thus provides a simple explanation for the abundance and old age of low-molecular-weight DOM[2–4]; whereas larger biopolymers are more likely to assemble to form stable POM gels, small polymers remain in the DOM pool owing to their low probability of stable assembly. As any kind of polymer shortening (physical, chemical or biological) decreases the chances of assembly into stable POM microgels, it will in general also reduce the accessibility to biodegradation. However, instead of increasing the bioavailability of organic matter, the formation of POM microgels could also have the opposite effect of preventing biodegradation: crystalline mineralization or phase-transition-induced condensation can turn POM microgels into refractory networks that may be more susceptible to removal from the water column through sedimentation (Fig. 4).

In the experimental conditions of this study, the assembly of DOM polymers results from collisions due to diffusional mobility. The influence on microgel assembly of physical (convectional or turbulent flows, high pressures, or low temperatures), chemical or biological factors, or the presence of longer chain polymers (in this case excluded by the 0.22-μm filtration), as found in the ocean, remains to be investigated. Although the detailed mechanisms giving rise to the transformation and degradation of marine organic matter remain controversial[3,4], the application of polymer gel physics promises to provide new answers. □

Methods

Water sampling and filtration. Seawater samples were collected in Puget Sound (WA, USA), the North Pacific and the Arctic. The samples were gravity filtered through a GF/F fibreglass membrane and a 0.22-μm Millipore tandem (pre-washed with 0.1 N HCl), transported to the laboratory in clean sealed bottles, and stored in the dark at 4 °C, for 1–6 weeks.

Particle sizing. The assembly of microgels was monitored by measuring particle size by both homodyne dynamics laser scattering and by flow cytometry. Seawater samples were shaken, and refiltered through a 0.22-μm Millipore membrane (pre-washed with 0.1 N HCl). Aliquots (10-ml) were then poured directly into scattering cells. The scattering cells were positioned in the goniometer of a Brookhaven laser spectrometer (Brookhaven Instruments, NY, USA). Polymer assembly was monitored for 10 d, by analysing the scattering fluctuations detected at a 45° scattering angle. The autocorrelation function of the scattering intensity fluctuations was averaged over a 10-min sampling time, using a Brookhaven BI 9000AT autocorrelator. Particle size distribution was calculated by the CONTIN method[30]. In parallel experiments, the polymer assembly was inhibited by chelating Ca^{2+} and Mg^{2+} by addition of 10 mM EDTA to the sea water. Control experiments were conducted in replicate samples containing 0.02% sodium azide to rule out microbial contamination. Measurements of microgel size were also performed in the same seawater samples, using a Coulter Epics Profile flow cytometer. In this case, the assembled gels were labelled with Nile red. Performance of these two particle sizing methods is complementary: whereas flow cytometry renders good estimates of large (>1 μm) particle size, DLS yields reliable sizing in the submicrometre range. Calibrations of both methods were conducted using standard monodipserse suspensions of latex microspheres ranging from 50 nm to 6 μm (Polysciences Inc., PA, USA).

Environmental scanning electron microscopy (ESEM). This powerful electron microscopy method enables materials—including living cells—to be studied at electron microscopy resolution (40 Å) while still fully hydrated. ESEM provides a non-destructive, non-invasive tool to investigate hydrated polymer networks in their native conformations. The present studies were conducted in assembled microgels retained on Millipore filters using an ElectroScan ESEM (model 2020, ElectroScan, MA, USA).

X-ray microanalysis. Microgels obtained by assembly of marine polymers from the DOM pool were fixed with a solution containing 0.5% glutaraldehyde, 0.25 M sucrose, and 0.1 M sodium cacodylate at pH 7.4, 20 °C. The samples were dehydrated in ethanol, and dried in fluorocarbon (Peltri II, Ted Pella, CA, USA). The specimens were sputter-coated with gold-palladium, and examined in a JEOL 840A (Japan) scanning electron microscope with energy dispersive spectroscopy capabilities.

Polymer gel phase transition. Swelling/condensation transitions were investigated at 20 °C by monitoring the volume changes of the microgels in sea water at pH ranging from 8 to 2.

Received 27 February; accepted 10 December 1997.

1. Hedges, J. I. Global biogeochemical cycles: progress and problems. *Mar. Chem.* **39,** 67–93 (1992).
2. Guo, L. & Santschi, P. H. Composition and cycling of colloids in marine environments. *Rev. Geophys.* **35,** 17–40 (1997).
3. Kepkay, P. E. Particle aggregation and the biological reactivity of colloids. *Mar. Ecol. Prog. Ser.* **109,** 293–304 (1994).
4. Amon, R. M. W. & Benner, R. Bacterial utilization of different size classes of dissolved organic matter. *Limnol. Oceanogr.* **41,** 41–51 (1996).
5. Wells, M. L. & Goldberg, E. D. The distribution of colloids in the North Atlantic and Southern Oceans. *Limnol. Oceanogr.* **39,** 286–302 (1994).
6. Cowen, J. P. & Holloway, C. F. Structural and chemical analysis of marine aggregates: in situ macrophotography and laser confocal and electron microscopy. *Mar. Biol.* **126,** 163–174 (1996).
7. Alldredge, A. L., Passow, U. & Logan, E. B. The abundance and significance of a class of large, transparent organic particles in the oceans. *Deep-Sea Res.* **40,** 1131–1140 (1993).
8. Benedetti, M. F., Van Riemsdijk, W. H. & Koopal, L. K. Humic substances considered as a heterogenous Donnan gel phase. *Environ. Sci. Techol.* **30,** 1805–1813 (1996).
9. de Gennes, P. G. & Leger, L. Dynamics of entangled polymer chains. *Annu. Rev. Phys. Chem.* **33,** 49–61 (1982).
10. Edwards, S. F. The theory of macromolecular networks. *Biorheology* **23,** 589–603 (1986).
11. Li, Y. & Tanaka, T. Phase transitions of gels. *Annu. Rev. Mater. Sci.* **22,** 243–277 (1992).
12. Stordal, M. C., Santschi, P. H. & Gill, G. A. Colloidal pumping: evidence for the coagulation process using natural colloids tagged with ^{230}Hg. *Environ. Sci. Technol.* **30,** 3335–3340 (1996).
13. Verdugo, P. Polymer gel phase transition in condension-decondensation of secretory products. *Adv. Polym. Sci.* **110,** 145–156 (1994).
14. Aluwihare, L. I., Repeta, D. J. & Chen, R. F. A major biopolymeric component to dissolved organic carbon in surface sea water. *Nature* **387,** 166–169 (1997).
15. Caswell, A. H. & Hutchison, J. D. Visualization of membrane bound cations by a fluorescent technique. *Biochem. Biophys. Res. Commun.* **42,** 43–49 (1971).
16. Katchalsky, A., Lifson, S. & Eisenberg, H. J. Equation of swelling for polyelectrolyte gels. *J. Polym. Sci.* **7,** 571–574 (1951).
17. Tam, P. Y. & Verdugo, P. Control of mucus hydration as a Donnan equilibrium process. *Nature* **292,** 340–342 (1981).
18. Crenshaw, M. A. in *Biological Mineralization and Demineralization* (ed. Nancollas, G. H.) 243–257 (Springer, Berlin, 1982).

19. Verdugo, P., Orellana, M. V. & Freitag, C. The secretory granule as a biomimetic model for drug delivery. *Proc. 22nd Int. Symp. on Controlled Release of Bioactive Materials* **22,** 25 (1995).
20. Marsh, M. E. Polyanion-mediated mineralization-assembly and reorganization of acidic polysaccharides in the Golgi system of a cocolithphorid algal during mineral deposition. *Protoplasma* **177,** 108–122 (1994).
21. Addadi, L., Moradian, J., Shay, E., Maraudas, N. G. & Weiner, S. A chemical model for the cooperation of sulfates and carboxylates in calcite crystal nucleation: relevance to biomineralization. *Proc. Natl. Acad. Sci. USA* **84,** 2732–2736 (1987).
22. Lubbers, G. W., Gieskes, W. W. C., del Castilho, P., Salomons, W. & Bril, J. Manganese accumulation in the high pH microenvironment of *Phaeocystis* sp. (Haptophyceae) colonies from the North Sea. *Mar. Ecol. Prog. Ser.* **59,** 285–293 (1990).
23. Morse, J. W. & Mackenzie, F. T. *Geochemistry of Sedimentary Carbonates* (Elsevier, Amsterdam, 1990).
24. Orellana, M. V. & Perry, M. J. An immunoprobe to measure Rubisco concentrations and maximal photosynthetic rates of individual phytoplankton cells. *Limnol. Oceanogr.* **37,** 478–490 (1992).
25. Benner, R., Pakulski, J. D., McCarthy, M., Hedges, J. I. & Hatcher, P. G. Bulk chemical characteristics of dissolved organic matter in the ocean. *Science* **255,** 1561–1564 (1992).
26. Mayer, L. M. Surface area control of organic carbon accumulation in continental shelf sediments. *Geochim. Cosmochim. Acta* **58,** 1271–1284 (1994).
27. Nishikawa, T., Akiyoshi, K. & Sunamoto, J. Supramolecular assembly between nanoparticles of hydrophobized olysaccharide and soluble protein complexation between the self-aggregate of cholesterol-bearing pullalan and α-chymotrypsin. *Macromolecules* **27,** 7654–7659 (1994).
28. Largeau, C. in *Role of Nonliving Organic Matter in the Earth's Carbon Cycle* (eds Zepp, R. G. & Sonntag, C.) 275–292 (Wiley, New York, 1995).
29. Kieber, R. J., Zhou, X. & Mopper, K. Formation of carbonyl compounds from UV-induced photodegradation of humic substances in natural waters; fate of riverine carbon in the sea. *Limnol. Oceanogr.* **35,** 1503–1515 (1990).
30. Provencher, S. W. A constrained regularization method for inverting data represented by linear algebraic or integral equations. *Comput. Phys. Commun.* **27,** 213–227 (1982).

Acknowledgements. We thank M. J. Perry, P. Jumars and J. Hedges for their comments and suggestions. This work was supported by the US NSF (Polar Program) and the Royalty Research Fund (University of Washington).

Correspondence should be addressed to P.V.

Influence of oxygen exposure time on organic carbon preservation in continental margin sediments

Hilairy E. Hartnett, Richard G. Keil, John I. Hedges & Allan H. Devol

School of Oceanography, Box 357940, University of Washington, Seattle, Washington 98195-7940, USA

Today, over 90% of all organic carbon burial in the ocean occurs in continental margin sediments[1]. This burial is intrinsically linked to the cycling of biogeochemically important elements (such as N, P, S, Fe and Mn) and, on geological timescales, largely controls the oxygen content of the atmosphere[2–4]. Currently there is a volatile debate over which processes govern sedimentary organic carbon preservation[5–8]. In spite of numerous studies demonstrating empirical relationships between organic carbon burial and such factors as primary productivity[9], the flux of organic carbon through the water column[10], sedimentation rate[11,12], organic carbon degradation rate[13], and bottom-water oxygen concentration[8,14], the mechanisms directly controlling sedimentary organic carbon preservation remain unclear. Furthermore, as organic carbon burial is the process that, along with pyrite burial[15], balances O_2 concentrations in the atmosphere, it is desirable that any mechanism proposed to control organic carbon preservation include a feedback buffering atmospheric oxygen concentrations over geological time. Here we compare analyses of sediments underlying two regions of the eastern North Pacific Ocean, one which has oxygen-depleted bottom waters and one with typical oxygen distributions. Organic carbon burial efficiency is strongly correlated with the length of time accumulating particles are exposed to molecular oxygen in sediment pore waters. Oxygen exposure time effectively incorporates other proposed environmental variables[8–14], and may exert a direct control on sedimentary organic carbon preservation and atmospheric oxygen concentrations.

Marine sediments and overlying waters were sampled during three cruises off Washington State and two cruises off the northwestern coast of Mexico. There is a prominent O_2-deficient zone over the Mexican margin between 150 and 600 m water depth (Fig. 1a) in which dissolved O_2 concentrations are often too low to detect by conventional techniques. In contrast, the Washington margin has a weaker O_2-minimum zone with concentrations decreasing to ~20 μmol l^{-1} at 800 m. Both margins have a range in sediment accumulation rates (see Table 1). Ocean-colour satellite images from the Coastal Zone Color Scanner suggest that throughout the year, the Mexican margin study-site has lower pigment concentrations (and by inference, lower primary production rates) than the Washington coast site. The sharp contrasts between these two regions help to distinguish factors affecting sedimentary organic carbon (OC) preservation. For example, if primary production is the controlling factor, the Washington margin should have a higher degree of OC preservation. Alternatively, if sediment accumulation rate is the controlling factor, deposits with similar accumulation rates should have comparable degrees of OC preservation in both regions. Finally, if length of oxygen exposure dictates the extent of preservation, then the Mexican margin should have a greater degree of OC preservation.

Sediment samples were taken along transects that ran perpendicular to the shore from depths of ~100–1,000 m. Organic carbon contents in Washington margin sediments were <2.0 wt%, whereas those on the Mexican margin were as high as 12.0 wt% (Fig. 1b). This difference alone suggests the strongly oxygen-deficient zone off the coast of Mexico increases OC preservation. Mexican slope sediments, which had the lowest overlying water oxygen concentrations, had higher OC burial rates and lower rates of OC oxidation than did inshore shelf sediments (Table 1). Washington slope sediments had lower rates of both OC oxidation and burial than did Washington shelf sediments. Although OC burial rates for the Washington and Mexican margins were roughly similar, OC oxidation rates on the Washington margin were up to a factor of five higher than for the Mexican margin.

Organic-carbon burial efficiency has been used as an indicator of the extent of OC preservation in sediments[10,12,16,17]. We define burial efficiency as the burial rate of OC below 15 cm, expressed as a

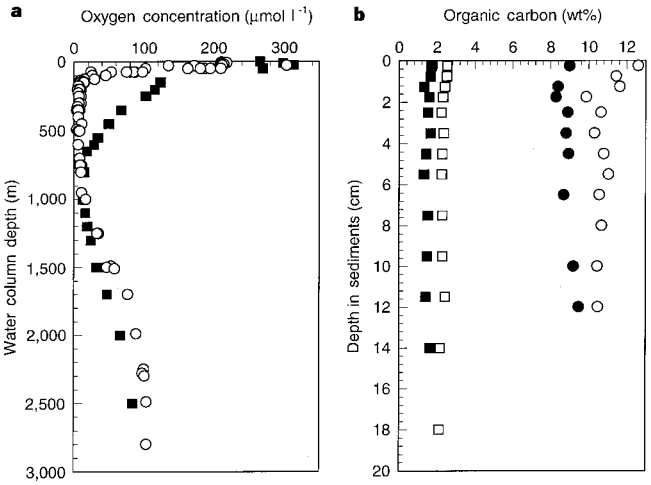

Figure 1 Water column O_2 and sediment carbon contents for study sites from the Washington and Mexican margins. **a**, Dissolved O_2 concentration as a function of water depth for the continental margins of Washington State (squares) and northwestern Mexico (circles). Note that the Mexican O_2 concentrations between 150 and 600 m depth are indistinguishable from zero. **b**, Weight per cent organic carbon as a function of depth in sediments for representative stations from the Washington (empty squares, 630 m; filled squares, 120 m) and Mexican continental margins (empty circles, 620 m; filled circles, 150 m).